

# Durable photocatalytic thin coatings for road applications

Julien G. Mahy <sup>a</sup>\*, Carlos A. Paez <sup>a</sup>, Jonas Hollevoet <sup>a</sup>, Luc Courard <sup>b</sup>, Elia Boonen <sup>c</sup>, Stéphanie D. Lambert <sup>a</sup>

<sup>a</sup> Department of Chemical Engineering - Nanomaterials, Catalysis & Electrochemistry, University of Liège, B6a, Quartier Agora, Allée du six Août 11, 4000 Liège, Belgium

<sup>b</sup> Department ArGENCo – Urban and Environmental Engineering, University of Liège, B52, Quartier Polytech, Allée de la Découverte 9, 4000 Liège, Belgium

<sup>c</sup> Belgian Road Research Centre (BRRC), Woluwedal 42, 1200 Brussels, Belgium

**\*Corresponding author:** Julien G. Mahy, Department of Chemical Engineering - Nanomaterials, Catalysis & Electrochemistry, University of Liège, B6a, Quartier Agora, Allée du six Août 11, 4000 Liège, Belgium. E-mail address: [julien.mahy@uliege.be](mailto:julien.mahy@uliege.be). Tel: +32 4 366 35 63.

**Keywords:** sol-gel process, TiO<sub>2</sub> film, photocatalytic concrete, NO<sub>x</sub> reduction, road application

## Abstract

In this study, 6 different coatings have been developed as photocatalytic coatings based on TiO<sub>2</sub>, which can be applied to concrete for road applications. The goal of these coatings is to degrade pollutants such as nitrogen oxides and volatile organic compounds emitted by road transport. The coatings are synthesized by sol-gel process in organic or water solvent or by a functionalization technique with hydroxybenzoic acid on commercial TiO<sub>2</sub> nanoparticles (P25). These suspensions are deposited by dip-coating or spray-coating on three different concrete substrates: pavement blocks, brushed or exposed aggregates road concrete. For each process, particular attention has been paid to the development of

TiO<sub>2</sub> synthesis that will be easily produced on a larger scale. The samples are characterized with photocatalytic test on NO<sub>x</sub> degradation, mechanical resistance test and resistance to freeze-thaw cycles in presence of de-icing salts. Except from the samples resulting from the sol-gel organic route, all other samples show a NO<sub>x</sub> degradation between 10 and 45 %. From resistance point of view, the best coating is the TiO<sub>2</sub> P25/E coating synthesized by functionalization of P25 nanoparticles. Results highlight that anatase TiO<sub>2</sub> is well present at the surface of the sample and an optimal TiO<sub>2</sub> loading exists for this coating. The TiO<sub>2</sub> P25/E coating shows promising properties for road applications.

## 1. Introduction

Environmental pollution is a global concern that engenders to develop new technologies and cleaner processes. Human is always responsible of many sources of environmental pollution. These can contaminate ecosystems and subsequently degrading air, terrestrial and aquatic environments as well as generating nuisances for life [1].

The atmospheric pollution is defined [2] as the presence in the atmosphere of certain pollutants (chemicals, particles, biological elements,...[3]) at levels having negative repercussions on human health, environment and cultural heritage like the buildings, monuments and equipments. This air pollution can come from natural or anthropogenic sources. Among human activities, combustion processes are the main sources of emission.

Pollutants emitted by road transport represent a non-negligible part of the global air pollution. The main components are nitrogen oxides (NO<sub>x</sub>), carbon dioxide (CO<sub>2</sub>), volatile organic compound (VOC) and particle matter (PM). NO<sub>x</sub> are serious pollutants causing production of tropospheric ozone, acid rains, global warming and human diseases, particularly respiratory and immune systems diseases [4]. So various legislations have been established to reduce their emissions by the road transport.

In addition to better vehicle design to reduce emission, some methods can be implemented to destroy NO<sub>x</sub> after emission. A possible one is photocatalysis [5]: this process uses a material (the photocatalyst) which degrade pollutant with a set of oxidation-reduction reactions when activated by light. The most

used photocatalyst is  $\text{TiO}_2$  [6,7] which is non-toxic, cheap and sensitive to Ultraviolet (UV) radiation with a band gap of 3.2 eV for its anatase phase [8,9].

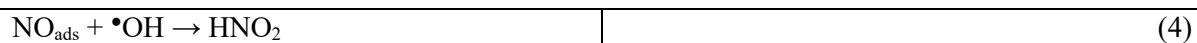
Because of its semi-conductivity, when the anatase  $\text{TiO}_2$  is exposed to an UV radiation of energy  $h\nu$ , these photons are absorbed and promote an electron ( $e^-$ ) of the valence band (VB) to the conduction band (CB) leaving a hole ( $h^+$ ) behind it (eq. 1) [6,10–12]:



The electrons are then transferred to oxidative molecules like  $\text{O}_2$  and the holes are transferred to reductive molecules like  $\text{H}_2\text{O}$  according to eq. 2 and 3 [6,10–12]:



The radicals produced in contact with  $\text{O}_2$  and  $\text{H}_2\text{O}$  are  $\text{O}_2^{\bullet-}$  and  $\bullet\text{OH}$  (eq. 2 and 3). These radicals react with pollutants to degrade them [6,10–12]. In the case of nitrogen oxide adsorbed (ads) at the surface of the catalyst, the mechanism is as follow [13–15]:



Nitric acid ( $\text{HNO}_3$ ) is then produced at the surface of the photocatalyst.

Due to the surface nature of the photo-oxidation reactions of NO, it is therefore necessary that the titanium dioxide must be present on the surface of the road to be efficient in the air depollution. Photocatalysis for road application consists of degrading pollutants emitted by the transport with  $\text{TiO}_2$  introduced into the road surface. Pollutants as well as water and oxygen are adsorbed at the road surface composed of photocatalytic concrete [16]. Under solar UV rays,  $\text{TiO}_2$  is activated and will produce radicals which will react with the adsorbed pollutants, such as  $\text{NO}_x$ , to transform them into less polluting substances which will be eliminated by washing or rain [16].

Currently, there are two major techniques to obtain photocatalytic concrete based on TiO<sub>2</sub> [16]. The first is to introduce the photocatalyst into the bulk of the pavement material. TiO<sub>2</sub> is usually incorporated into the upper layer of the road pavement or into a layer placed at the surface of the road cover. This type of implementation in the mass has the advantage of making appear new particles of TiO<sub>2</sub> on the surface of the top layer when it wears under the traffic. However, only surface TiO<sub>2</sub> has access to light and pollutants, and so only this part is active. The remainder of deeper TiO<sub>2</sub> is not active and therefore constitutes a loss and increases the initial cost.

The second technic consists to spray TiO<sub>2</sub> suspension (coating) on road surfaces [17]. This technique has the advantage to use less TiO<sub>2</sub>, which reduces the cost. Moreover, this method makes it possible to process existing roads, most of the TiO<sub>2</sub> is on the surface and will therefore be active. On the contrary, since the photocatalytic material is on the surface, the abrasion may decrease the adhesion of TiO<sub>2</sub> particles over time and thus the durability of the coating [16,18].

Several studies have been made to assess the possibility to use TiO<sub>2</sub> on road application to reduce pollution. For examples, in Antwerp in Belgium [16], photocatalytic pavements were used for path lanes. In this case, TiO<sub>2</sub> is incorporated into the upper layer of the pavement blocks (first technique). In The Netherlands [16], photocatalytic concrete coating was used to reduce the amount of greenhouse gases and depollute the air. TiO<sub>2</sub> coatings have also been applied in tunnels [19,20] equipped with UV lamps in order to reduce NO<sub>x</sub> concentration; as tested in Rome and Brussels [16,19,20].

Concrete is composed of aggregates, sand, cement, water and admixtures with specific functions [21]. Mechanical strength of the concrete depends on the concrete composition and the (inert) aggregate skeleton which can also have an influence on the appearance of the concrete [21]: it is also correlated to appropriate mix design and proper water/cement ratio, with regard to the type of application and the environmental conditions.. Cement is a hydraulic binder which links the different constituents of the concrete by means of a chemical reaction with water. This will induce cohesion of the mix and development of compressive strength [21].

TiO<sub>2</sub> suspension can be obtained with different synthesis and processes. For several years, sol-gel synthesis has proven to be effective for the synthesis of metallic oxides such as TiO<sub>2</sub>, SiO<sub>2</sub>, SnO<sub>2</sub>, Al<sub>2</sub>O<sub>3</sub>,... in the form of powders or films with control of the nanostructure and surface properties [9,22–

27]. The sol-gel process is called “soft chemistry” because reactions occur at low temperature and low pressure. In the case of the formation of  $\text{TiO}_2$  network, the titanium precursor undergoes two main reactions: hydrolysis and condensation (Eqs. 7 and 8) [28].

$\text{Ti-(OR)}_4 + \text{H}_2\text{O} \rightarrow (\text{OR})_3\text{-Ti-OH} + \text{ROH}$	(7)
$(\text{OR})_3\text{-Ti-OH} + \text{HO-Ti-(OR)}_3 \rightarrow (\text{OR})_3\text{-Ti-O-Ti-(OR)}_3 + \text{H}_2\text{O}$	(8)

where R is an alkyl group (-CH<sub>3</sub>, -C<sub>2</sub>H<sub>5</sub>, -CH(CH<sub>3</sub>)<sub>2</sub>,...)

By controlling the rate of these reactions, a liquid sol can be obtained. In order to obtain  $\text{TiO}_2$  by sol-gel processes, two paths can be considered depending on the solvent used: non-aqueous and aqueous routes. In a non-aqueous process, the sol-gel synthesis is conducted in an organic solvent able to complex the titanium precursor ( $\text{Ti-(OR)}_4$ ) to control its reactivity. A stoichiometric amount of water is added to avoid precipitation [23,29–31]. The material then undergoes a drying and calcination step to remove residual organic molecules and to crystallize amorphous  $\text{TiO}_2$  in anatase or rutile phases [32]. In an aqueous process, water is the solvent and is present in large excess. In this synthesis, peptizing agents are used to form small  $\text{TiO}_2$ -anatase nanoparticles at low temperature (< 100°C) [8,33–37]. The main advantages of this route are that water is used as the solvent and anatase phase is obtained at low temperatures. This method is thus well suited for industrialization [11].

Another way to produce  $\text{TiO}_2$  suspension is to disperse a  $\text{TiO}_2$  powder in a solvent in specific conditions in order to obtain a stable suspension [38].

The aim of this work is to develop photocatalytic coatings based on  $\text{TiO}_2$ , which can be applied to concrete for road applications. The goal of these coatings is to degrade pollutants such as nitrogen oxides and organic compounds emitted by road transport. Particular attention has been paid to the development of  $\text{TiO}_2$  suspensions that will be easily produced on a larger scale. Three types of concrete substrates will be used, brushed and exposed aggregates road concrete, and pavement blocks. This work is composed of 4 main steps: (i) development of  $\text{TiO}_2$  suspension using either the sol-gel synthesis in aqueous and organic solvent, or a patented method concerning the functionalization of a commercial  $\text{TiO}_2$  powder (P25) and a Degussa patent; (ii) coating deposition with dip- or spray technics; (iii) characterizations of the coatings with photocatalytic test on  $\text{NO}_x$  degradation, mechanical resistance test and resistance to freeze-thaw cycles in the presence of de-icing salts ; (iv) characterization of the

best coating by SEM and X-ray diffraction measurements, profilometry and photocatalytic test on NO<sub>x</sub> degradation.

## 2. Materials and methods

### 2.1. Concrete manufacture

The road concrete with brushed or exposed aggregates surface finish was provided by the Belgian Road Research Centre (BRRC) with use of cement type CEM III/A 42,5 N LA. The brushed concrete is obtained by brushing the surface with a bristle brush. A third substrate is used to apply a photocatalytic coating: pavement blocks manufactured by the Coeck Company. All samples are cut to a size of 10 x 5 cm<sup>2</sup> and thickness of 7 (road concrete) or 2,5 (pavement blocks) cm.

The concrete porous surface property was estimated by measuring the polyethylene glycol (Arcos Organics, average M. W. 200) amount introduced in the sample after 24 h in solution. For each substrate, 5 measurements (on 5 samples) were made in order to obtain a representative value of the porous volume. It allowed to know the accessible porous volume for the coating solution.

### 2.2. TiO<sub>2</sub> suspensions

4 processes will be used to produce TiO<sub>2</sub> suspensions: an aqueous and an organic sol-gel synthesis, a patent using the functionalization of Degussa P25 and a patent from Degussa.

#### 2.2.1. Aqueous TiO<sub>2</sub> sol-gel suspension

The reagents are titanium (IV) tetraisopropoxide (TTIP ≥ 97%, Sigma-Aldrich), nitric acid (HNO<sub>3</sub>, 65%, Merck), isopropanol (IsoP, 99.5%, Acros) and distilled water. 1 L of distilled water is acidified by HNO<sub>3</sub> to a pH equal to 1. Then, 134.4 g of TTIP is added to 47.2 g of IsoP, the mixture is stirred at room temperature for 30 min. The TTIP-IsoP mixture is added to acidified water under vigorous stirring. The solution stays under stirring for 4 h at 80 °C. After this time, a light white-blue

transparent liquid sol is obtained and kept in ambient atmosphere [11,39]. Coating with this colloid is called  $\text{TiO}_2$  AQ.

#### 2.2.2. Organic $\text{TiO}_2$ sol-gel suspension

The reagents are titanium (IV) tetraisopropoxide (TTIP  $\geq$  97%, Sigma-Aldrich), methoxyethanol (methoxyethanol ACS 99.3+%, Alfa Aesar) and deionised water. 7.79 mL of TTIP is added to one half of the solvent, 48 mL, and vigorously stirred for 30 min in a first vessel. In a second vessel, a small amount of deionised water, 1.16 mL, is dissolved in the second half of solvent, 48 mL. After 30 min of stirring, the water containing solution is added to the first vessel in order to induce the hydrolysis and condensation reactions and the final mixture is stirred vigorously for 1 h. Stable colloidal suspensions suitable for film deposition are obtained [40]. Coating with this colloid is called  $\text{TiO}_2$  ORGA.

#### 2.2.3. Functionalization patent $\text{TiO}_2$ P25 suspension

The complete process is described in [38]. It consists in a surface functionalization of a commercial  $\text{TiO}_2$  powder (Degussa P25) with hydroxybenzoic acid producing stable colloid in water or ethanol solvent. Coatings with this colloid are called  $\text{TiO}_2$  P25/W if water is the solvent and  $\text{TiO}_2$  P25/E if ethanol is the solvent. In these colloids, P25  $\text{TiO}_2$  is complexed by the hydroxybenzoic acid grafted at the surface leading to a better repulsion between the particles [38,41,42]. The hydroxybenzoic acid is grafted to the  $\text{TiO}_2$  with its carboxylic acid function and its phenyl group is directed towards the solvent [38,41,42].

#### 2.2.4. Degussa patent suspension

These suspensions are produced from a Degussa patent [43]. 120 g of P25  $\text{TiO}_2$  is mixed in 300 mL of water. NaOH (0.01 M) is used to adjust the *pH* to 6.2. Then 150 mL of this mixture is added to

100 mL of water or to 100 mL of ethanol. Coatings with this colloid are called TiO<sub>2</sub> Degussa/W if only water is the solvent and TiO<sub>2</sub> Degussa/E if ethanol is present.

So 6 suspensions are produced with 4 different processes.

### 2.3. Deposition methods

Two methods are used to coat concrete samples: dip coating and spray coating.

For dip-coating, as this technic is not possible for road concrete, only paving blocks are coated by this method. The method consists in depositing the substrate, with its face to be treated downwards, in a plastic box containing 40 mL of the solution to be applied. In the container, the sample is raised about 1 mm so that the solution is in contact with the surface to be treated. During application, one plastic cover is placed on the container to avoid evaporation of the solvent. This soaking is carried out for 30 min, then the sample is dried at 50 °C.

For the spray-coating, this technic consists to spray the TiO<sub>2</sub> suspensions at the surface of the samples. The amount of TiO<sub>2</sub> deposited is maintained constant between the samples to 6.67 g of TiO<sub>2</sub>/m<sup>2</sup>. For each substrate, it represents theoretically 170 nm of TiO<sub>2</sub> coating. The spray is placed at 7 cm of the surface to coat and go along the sample until the tank is empty of suspension. The time between 2 passings is 10 sec with ethanol solvent or 30 sec with water. Samples are then dried at 50 °C.

### 2.4. Photocatalytic tests

The photocatalytic activity of samples is tested on the global decrease of NO<sub>x</sub> in a polluted air containing initially only NO according ISO 22197-1 [44]. Indeed, NO<sub>2</sub> is produced during NO degradation (Equation 5). So the efficiency of NO<sub>x</sub> is defined as:

NO <sub>x</sub> removing = removed NO – formed NO <sub>2</sub>	(9)
--	-----

During the test, the coated samples are placed in a sealed piston reactor using quartz glass in order to minimize the absorption of UV radiation by the glass. This device is shown in Figure 1. The

position of the sample in the reactor is such that there is a vacuum of  $5 \pm 0.5$  mm between the surface of the samples and the glass. This section of the gas must be low to avoid mixing phenomena and to have fixed conditions in the reactor. A light source of wavelength between 300 and 400 nm irradiates the sample with UV-A radiation and the luminous intensity received by the surface of the sample is  $10 \pm 0.5$  W/m<sup>2</sup>. This intensity is measured using a LT Lutron UVA-365 radiometer. Wet air (RH = 50%) containing 1000 ppb of NO passes over the surface of the sample with a flow rate of  $3 \pm 0.15$  L/min and then passes through a NO<sub>x</sub> analyzer. The analyzer used is the NO<sub>x</sub> ANALYZER-T200 model of Teledyne Advanced Pollution Instrumentation. This device is able to continuously measure the quantity of NO, NO<sub>2</sub> and therefore NO<sub>x</sub> at output of the reactor. Finally, it should be noted that the relative humidity in the reactor must be of 50% and the temperature is  $25 \pm 2.5^\circ$  C.

The procedure consists to illuminate the sample using UV-A lamp for 1 h and measure the variation of the NO and NO<sub>2</sub> concentrations at the reactor outlet. After this time, the UV lamp is switched off and the NO concentration rises to its initial value. When the NO concentration is stabilized around 1000 ppb in the reactor, the lamp UV is switched on again for 1 h to measure the change in concentration of the NO<sub>x</sub> in the air passing over the sample. The lamp is then switched off and the concentration of NO stabilizes at its initial value which marks the end of the test.

With this test, the specific yield of desorption of NO<sub>2</sub> is also calculated. It represents the amount of NO<sub>2</sub> produced by NO degraded (eq. 10). If it is equal to 0, no NO<sub>2</sub> is present in the outlet of the reactor and if it is equal to 1, all NO is transformed in NO<sub>2</sub> and the total NO<sub>x</sub> reduction is zero.

$$\eta_{NO_2} = \frac{NO_2_{Produced}}{NO_{degraded}} \quad (10)$$

## 2.5. Kinetics

Following the photocatalytic degradation of NO, it is possible to calculate the kinetic constant of the reaction assuming that it is of the first order. This constant will allow to compare the performances of the different coatings on the different substrates. The first order kinetic constant [45],  $k$  [m/s], is determined by mass balance on an infinite slice of the piston reactor. This value has the advantage,

compared to the kinetic constant  $k'$  [1/s], to be related to the surface unit of the substrate which will make it possible to compare the different substrates with one another independently of their real surface.

The mass balance on the volume,  $dV$ , is shown on Figure 2.

In Figure 2,  $C_0$  [mol/m<sup>3</sup>] is the input concentration in NO,  $\bar{V}_0$  [m<sup>3</sup>/s] is the volumetric flow of gas at the inlet and  $C_s$  [mol/m<sup>3</sup>] is the NO exit concentration. On the right-hand side of Figure 2,  $\bar{V}$ ,  $C$  and  $f$  represent respectively the volumetric flow [m<sup>3</sup>/s], the concentration of NO [mol/m<sup>3</sup>] and the conversion rate [-] at the inlet of the element of volume  $dV$  [m<sup>3</sup>], which has a contact surface with the sample of surface  $dS$  [m<sup>2</sup>]. At the exit of this slice of infinitesimal thickness, these quantities are respectively  $\bar{V} + d\bar{V}$ ,  $C + dC$  and  $f + df$ . Assuming a steady state, the material balance on the volume  $dV$  is written:

$0 = C\bar{V} - (C + dC)\bar{V} - rdS$	(11)
--	------

$0 = -dC\bar{V} - kCdS$	(12)
-------------------------	------

where  $r = k C$  is the first order degradation rate of NO [mol/m<sup>2</sup>s] and  $k$  is the constant of the first order [m/s]. Knowing that the molar flow rate of gas  $F$  [mol/s] is equal to  $F = C V$ , this equation is simplified as following :

$dF = -kCdS$	(13)
--------------	------

Moreover, since  $F = F_0 * (1 - f)$ ,  $dF = -F_0 df$  and having  $C = C_0 (1 - f)$  where  $f$  (the conversion) is defined as  $\frac{C_0 - C}{C_0}$  with  $C_0$  and  $C$  are respectively the initial and current concentrations of the key component, the equation (13) becomes:

$F_0 df = kC_0(1 - f)ds$	(14)
--------------------------	------

$\frac{F_0 df}{C_0(1 - f)} = kds$	(15)
-----------------------------------	------

By integrating:

$\bar{V}_0 \ln \left( \frac{1}{1-f} \right) = kS$	(16)
---	------

At steady state  $\bar{V}_0 = \bar{V}$ :

$k = \frac{\bar{V}}{S} \ln \left( \frac{1}{1-f} \right)$	(17)
--	------

This equation allows calculating  $k$  for the different samples tested in this work.

## 2.6. Abrasion resistance test

The Polish Stone Value (PSV) device [46] – normally used to test aggregates – is used for applying a rolling load on test pavements on which the different coatings are applied by spray-coating according to section 2.3. The NO degradation will be measured, according to section 2.4, before and after the passage of samples in the PSV apparatus to evaluate the decrease of photocatalytic activity after simulation of abrasion by road traffic.

The PSV apparatus used is shown in [47]. The "road" wheel makes it possible to have 14 samples on its surface and a lever arm fitted with a weight makes it possible to apply, with a force of  $725 \pm 10$  N, the rubber wheel on the surface of the road wheel. Both wheels are rotated around their axis, the road wheel rotating at a speed of  $320 \pm 5$  rpm. During rotation, a mixture of water and particles is fed between the two wheels during  $180 \pm 1$  min to increase the friction between both surfaces. The particles are fed at a rate of  $3 \pm 1$  g/min and water at this double rate. Finally, the samples are recovered and washed to remove the small particles present on their surface. After drying, the photocatalytic activity of the samples is evaluated.

In order to be able to place the samples on the road wheel, these are prepared in slightly curved molds provided for this purpose. The concrete is the same as in section 2.1 but it was shaped in order to fit the sample older of the PSV apparatus. These samples had no specific surface finished (not brushed or granulated).

## 2.7. Freeze-thaw test with de-icing salts

This test is inspired by the CEN/TS 12390-9 standard [48]. To carry out the freeze-thaw test, the lateral faces of the test pieces are covered with epoxy resin (AKEPOX 1005) to prevent water infiltration by these faces. The resin is cured in an oven at 30 °C and then the samples are placed with their upper face downwards in a plastic box containing deionized water. The receptacle is closed with a plastic film to prevent the evaporation of water. This soaking, allowing the saturation of the test specimens, are prepared for 4 days.

Following this saturation, the deionized water is replaced by a saline solution prepared by dissolving 30 g of NaCl (VWR) in 970 g of deionized water. This solution aims to model the de-icing salts applied on roads. Containers containing test samples placed in the saline water are then introduced into a chamber allowing simulation of freeze and thaw cycles. Again, the containers are covered with a plastic film to prevent the evaporation of water. The temperature of the chamber is regulated by a probe placed in one of the containers. A freeze-thaw cycle lasts for 24 h and the temperature profile is shown in Figure 3.

## 2.8. Additional characterizations

For the best coating selected in this work, additional characterizations are realized. Microstructures and morphologies are investigated using FEG-ESEM XL30 of FEI scanning electronic microscope (SEM) at an acceleration voltage of 15 kV. This device is also equipped with an Energy Dispersive X-ray Spectrometry (EDX) allowing the elementary analysis of the sample.

X-ray diffraction-patterns are recorded with a Siemens D5000 powder diffractometer (Cu- $K\alpha$  radiation).

Pictures of the surface are also taken by profilometry (Veeco Dektak 8 Stylus Profile) with a magnification of 185 $\times$ .

The influence of the  $\text{TiO}_2$  loading in the coating on the photocatalytic activity is studied. For this purpose, the best coating is applied by spraying on the brushed concrete samples at various loads: 2  $\text{g/m}^2$ , 4  $\text{g/m}^2$ , 6.67  $\text{g/m}^2$  and 12  $\text{g/m}^2$ . Then the photocatalytic activity of these samples are measured according to section 2.4 to determine the optimal amount of  $\text{TiO}_2$  to apply and the influence of the  $\text{TiO}_2$  loading on the photocatalytic efficiency.

The assumption of the first order for the photocatalytic degradation of NO is checked on the best sample. Indeed, the kinetic is first order if, by plotting the reaction rate as a function of different initial NO concentration (250, 500, 750 and 1000 ppb), a linear curve is obtained.

### 3. Results and discussion

#### 3.1. Colloids and coatings

From the 4 processes, 6  $\text{TiO}_2$  colloids are obtained.  $\text{TiO}_2$  ORGA suspension is light yellow and transparent, while for the other suspensions a white-blue aspect is obtained. In all cases, colloids are stable *i.e.* no decantation is observed after 3 days. These sols can be coated on pavements with dip-coating and sprayed on brushed concrete, exposed aggregates concrete concrete and also pavement. As all suspensions are low viscous, spray-deposition is easy. Different aspects are obtained depending the coating technic. With dip-coating technic on pavement: (i) with  $\text{TiO}_2$  AQ and  $\text{TiO}_2$  ORGA, crystals are formed at the surface of the pavement and seem weakly anchored in the matrix; (ii) the other coatings are homogenous. Figure 4a illustrates the formation of crystals at the surface of the pavement for the  $\text{TiO}_2$  AQ suspension. For both  $\text{TiO}_2$  AQ and  $\text{TiO}_2$  ORGA, the XRD patterns of the crystals are measured and are represented on Figure 4b. For  $\text{TiO}_2$  AQ, anatase phase is detected with a small fraction of brookite phase, as reported with this type of synthesis [11,25,49]. For  $\text{TiO}_2$  ORGA, no peak associated to crystalline species is detected, this material will not be photoactive (section 3.3).

For the suspension used for the dip-coating, the stability, the amount of absorbed  $\text{TiO}_2$  and the pH are measured before and after deposition in order to obtain information about the concrete substrate influence, all these values are denoted in Table 1 ( $\text{TiO}_2$  ORGA is not taken into account as no crystalline

material is obtained). The amount of  $\text{TiO}_2$  absorbed (and so deposited) is related to the evolution of the volume of the remaining solution after the dip-coating process. Table 1 shows that the pH is modified after the contact with the pavement, as concrete is a basic solid, the pH increases in all cases. This increase of pH modified the stability of the colloids as the pH modification changes the surface charge of the particles. All colloids in water precipitate (Table 1), while these in ethanol stay stable. The amount of  $\text{TiO}_2$  deposited can be related to the stability of the colloid. Indeed, when the sols are stable, the  $\text{TiO}_2$  suspension can diffuse in the pavement and deposit in the open porosity leading to a bigger  $\text{TiO}_2$  deposition. When the colloid precipitates, the particles form aggregates which can block the open porosity of the pavement substrate, the amount of  $\text{TiO}_2$  deposited is so lower. For  $\text{TiO}_2$  AQ, the very low amount of  $\text{TiO}_2$  deposited can be probably linked to the difference of acid-base character of the suspension and the pavement. As this colloid needs a very acidic medium to be stable, the contact with the basic concrete produces a direct precipitation with low diffusion in the open porosity and agglomeration at the surface (crystal formation).

With spray coating, all samples are homogenous with a surface a little lighter than without coating.

### 3.2. Concrete substrates

The open porosity of the concrete substrate are denoted in Table 2. Different values are obtained depending the substrate, the ranking is as follows: pavement > brushed concrete > exposed aggregates concrete > mechanical test concrete substrate. This ranking can be also deduce from macroscopic observation of the substrate. Indeed, the mechanical test concrete substrate seems very dense, has a very smooth surface and no macroscopic pore. Contrarily, the pavements have a lot of macroscopic pores and the surface is quite rough like sands. The brushed and exposed aggregates concretes have intermediate porosity, when the aggregates are exposed the porosity decreases as the aggregates seem very dense. These different open porosities can be related to the photocatalytic activity (see section 3.3).

### 3.3. Photocatalytic activity on $\text{NO}_x$ degradation

The activity for all coatings on the different substrates are given in Table 3. This Table is divided in 3 parts: (i) the percentage of NO degradation (%), (ii) the specific yield of production of  $\text{NO}_2$  ( $\eta_{\text{NO}_2}$ ) and (iii) the global percentage of  $\text{NO}_x$  degradation (%).

The first part of Table 3 shows that the percentage of NO reduction varies depending on coatings, substrates and application methods. The most important degradation is achieved with the  $\text{TiO}_2$  P25/E sample which gives a mean decrease of 56 % of NO. Then comes  $\text{TiO}_2$  P25/W sample, which has an average reduction of 47 % of NO. The  $\text{TiO}_2$  AQ solution applied to the pavement by dip-coating presents a low degradation of NO equal to 7 %. This is probably due to the fact that when dipping the solution, the penetration of  $\text{TiO}_2$  into the surface porosity of the substrate is limited (crystals formation due to precipitation).  $\text{TiO}_2$  ORGA coating on pavement blocks with dip-coating degrades only an amount 0.4 % of NO present in the feeding. This amount being the same order as the variation of the NO concentration in the reactor feed, thus the NO reduction by  $\text{TiO}_2$  ORGA coating on pavement blocks is considered equal to 0 %. This is probably due to the fact that to obtain  $\text{TiO}_2$ -anatase (photocatalytic phase of  $\text{TiO}_2$ ) by this sol-gel method, a heat treatment at 300 °C is necessary [40] but has not been realized in this case. As an inactive phase is obtained with this coating, the activity is equal to zero for all samples coated with this solution.

Concerning specific yield of desorption of  $\text{NO}_2$  (Table 3), the presence of  $\text{NO}_2$  in the eluent of the reactor indicates that the photocatalytic reaction of NO with  $\text{TiO}_2$  passes through a stage of production of  $\text{NO}_2$ . First, a certain amount of the produced  $\text{NO}_2$  is desorbed from the  $\text{TiO}_2$  surface and is carried away by the gases. Secondly, it is assumed that another part of the  $\text{NO}_2$  remains adsorbed on the  $\text{TiO}_2$  surface to complement the reactions mechanism presented in Equations 4, 5 and 6. More the specific yield of  $\text{NO}_2$  is close to 0, more the degradation of NO is important compared to the amount of desorbed  $\text{NO}_2$ .

The  $\text{TiO}_2$  coatings show  $\eta_{\text{NO}_2}$  values varying from 0.26 to 1. The  $\text{TiO}_2$  ORGA and  $\text{TiO}_2$  AQ sols applied by dip-coating (dipped pavement in Table 3) present  $\eta_{\text{NO}_2}$  values equal to 1, which means that the decrease in the concentration of NO is entirely compensated by the desorption of an equal amount of  $\text{NO}_2$ . The dip-coated pavement blocks generally have a specific yield of desorption higher

than those for sprayed substrates. This may be due to the fact that during soaking, the substrate is in contact with a much larger amount of coating (Table 3) and during longer times than when applied by spray-coating. Therefore, soaking modifies the surface chemistry of the samples and the properties of adsorption of  $\text{NO}_2$  due to larger amount of  $\text{TiO}_2$  at the surface of the samples. Furthermore in Table 3,  $\eta_{\text{NO}_2}$  value for the sprayed specimens are the highest when the substrate is a paving block ( $\eta_{\text{NO}_2}$  average = 0.45) followed by the exposed aggregates ( $\eta_{\text{NO}_2}$  average = 0.38) and the brushed concrete ( $\eta_{\text{NO}_2}$  average = 0.34). This observation would indicate that the structure and chemical composition of the surface substrate have an influence on the adsorption and desorption of  $\text{NO}_2$  during the reaction mechanism. Indeed, the open porosity of the substrates are quite different (Table 2), the highest porous substrate is the pavement which leads to the highest  $\text{NO}_2$  desorption. So, this substrate has the maximal adsorption capacity and also the maximal possible desorption capacity.

Concerning the global percentage of  $\text{NO}_x$  degradation, the ultimate aim is to reduce the concentration of  $\text{NO}_x$  in air. Nevertheless, the above results have shown that the decrease in the concentration of NO is always accompanied by a desorption of a certain amount of  $\text{NO}_2$ . The best  $\text{TiO}_2$  coating will be the one, which presents the most significant decrease of NO while emitting the least  $\text{NO}_2$ , which corresponds to the coating leading to the largest reduction of  $\text{NO}_x$ . The average  $\text{NO}_x$  reduction percentages calculated on the basis of the two illumination cycles are given in Table 3.

It is the colloid  $\text{TiO}_2$  P25/E which generates the highest reduction of  $\text{NO}_x$  when the application is carried out by spray-coating. This coating is also the one with the largest NO reduction (56 % in Table 3). In fact in this study, such as  $\eta_{\text{NO}_2}$  values for the different coatings are generally of the same order, the more the reduction of NO is important, the more the degradation of  $\text{NO}_x$  will be significant. The colloid  $\text{TiO}_2$  P25/W presents the second best value for photoactivity.

This better activity for the  $\text{TiO}_2$  P25/E and  $\text{TiO}_2$  P25/W colloids can be explained by the surface modification of the P25 during the preparation of the colloid. Indeed, 4-hydroxybenzoic acid molecules have been grafted at the surface of the P25 allowing the production of stable colloids. Moreover, these new chemical groups can interacted with the surface of the concrete substrate to increase the adherence of the coating [38,41,42]. This good adherence of the  $\text{TiO}_2$  coating can lead to a

higher amount of the  $\text{TiO}_2$  deposited. Indeed, with the dip-coating samples (Table 1), the amount of  $\text{TiO}_2$  deposited is the higher with both colloids. The better activity for the colloid  $\text{TiO}_2$  P25/E compared to colloid  $\text{TiO}_2$  P25/W can be linked to the solvent used as ethanol spreads easily on the concrete substrate than water as this phenomenon can be observed when a drop of these two solvents is deposited at the surface of a concrete substrate (Figures 5a vs. 5b).

From the photocatalytic experiments, for a same colloid deposited on the different substrates, the brushed concrete seems to be the substrate which gives the highest  $\text{NO}_x$  degradation in nearly each colloid. This observation can be linked to the open porosity of the concrete substrate. Indeed, brushed concrete has an open porosity of  $0.016 \text{ g/cm}^3$ , which is the intermediate porous value compared to the other substrates. The concrete substrate needs sufficient porosity to have a high surface of contact between the  $\text{TiO}_2$  and the  $\text{NO}_x$  pollutant but the  $\text{TiO}_2$  needs to be exposed to the light to be active. If the porosity is too high or sinks too much in the concrete, the pores can be filled with  $\text{TiO}_2$  or not easily exposed to light. So, the porosity of the brushed concrete seems to be an optimal amount.

By assuming a first order reaction, kinetics constants are calculated for the two degradation reactions of  $\text{NO}$  and  $\text{NO}_x$  and the results are presented in Table 4. The kinetic constants,  $k_{\text{NO}_x}$ , are smaller for the degradation of  $\text{NO}_x$  because the desorption of  $\text{NO}_2$  is taken into account. From these results, the best coating is  $\text{TiO}_2$  P25/E.

### 3.4. Mechanical abrasion resistance and freeze-thaw test

To assess the mechanical abrasion resistance and the freeze-thaw resistance of the coatings, the residual photoactivity on the  $\text{NO}_x$  degradation is performed on the samples after these two tests. As the  $\text{TiO}_2$  ORGA coating has no activity, these tests are not carried out on this coating. Tables 3 and 4 gives the activity for each sample after the abrasion and freeze-thaw tests respectively. The surface of the samples is also observed and compared to the initial one.

For the abrasion resistance, a high decrease of photoactivity is observed on all coatings (Table 5). In this case, the concrete substrate was shaped in order to fit the sample older of the PSV apparatus. These samples had no specific surface finished (not brushed or granulated) and presents no open porosity

(Table 2). So, the amount of  $\text{TiO}_2$  exposed to the light is lower than with other substrates leading to lower photocatalytic activity.

Only sample  $\text{TiO}_2$  P25/E keeps an activity of 3% of  $\text{NO}_x$  degradation after the abrasion test. This coating has the highest adherence due to the hydroxybenzoic acid groups grafted at the surface of the P25 (section 3.3). Indeed, this molecule allows a better adherence between P25 and the concrete [38,41,42]. This test is very severe for the samples as all the surface is subject to the rolling abrasion, which is not the case on a real road application where some parts are less subject to vehicular traffic.

For the freeze-thaw test (Table 6), all substrates present macroscopic modifications of the surface, which can lead to loss of the surface coating. Indeed the coatings on brushed concrete and the aqueous sol-gel coating ( $\text{TiO}_2$  AQ) have not resisted to the freezing test with the consequence that the activity decreases to zero (Table 6). For the other substrates, a photocatalytic activity is maintained but reduced. Comparisons between coated and non-coated substrates show similar degradation of the surface, so the  $\text{TiO}_2$  coatings do not modify the resistance of these concretes to freeze-thaw tests. The colloids prepared in ethanol ( $\text{TiO}_2$  P25/E and  $\text{TiO}_2$  Degussa/E) are more resistant to the freeze-thaw test than these prepared in water. Indeed, residual water in the coatings can damage during the freeze-thaw cycle.

Regarding the photoactivity (Tables 1 and 2) and the resistance tests (Tables 3 and 4),  $\text{TiO}_2$  P25/E coating seems to be the best candidate for further characterizations.

### 3.5. Additional characterizations on $\text{TiO}_2$ P25/E coating

Figure 6 represents a SEM picture of the pavement block with and without the coating  $\text{TiO}_2$  P25/E. No major differences are observed between the two pictures. This is why an EDX analysis is made to identify the presence of  $\text{TiO}_2$ , the spectrum obtained is represented on Figure 7. For the blank pavement block, the main elements of the concrete are observed [21]: calcium, oxygen, sodium, aluminum, silicon and iron. For the  $\text{TiO}_2$  P25/E coated pavement block, titanium is observed further the elements of concrete. This analysis shows that  $\text{TiO}_2$  is well deposited on the surface of the sample.

An XRD measurement is made to evaluate the crystalline phase of  $\text{TiO}_2$  coating. Figure 8 shows the XRD pattern for the blank concrete in the  $[5^\circ, 60^\circ]$   $2\theta$  zone and Figure 9 shows the XRD pattern for the blank and the  $\text{TiO}_2$  P25/E coated pavement block with a zoom of 25x on the  $[24^\circ, 26^\circ]$   $2\theta$  zone, which corresponds to the peak of  $\text{TiO}_2$  anatase [8, 9]. For the blank concrete, the main crystalline phases of its components are present [21]: quartz ( $\text{SiO}_2$ ), calcium carbonate ( $\text{CaCO}_3$ ), calcium oxide ( $\text{CaO}$ ), rutile  $\text{TiO}_2$  at  $27.45^\circ$  and feldspath at  $28^\circ$  [50,51]. Concerning the coated sample, the same peaks are observed but a peak corresponding to anatase  $\text{TiO}_2$  is observed at  $25.3^\circ$  (Figure 9). This peak could be attributed to the  $\text{TiO}_2$  P25/E coating, which is composed of Degussa P25.

The pavement block is also observed with profilometry (Figure 10). A different surface is observed with the coating leading to a bright surface, the coating is well present at the surface of the pavement block.

A study of the optimal loading of  $\text{TiO}_2$  in the coating is made with a  $\text{TiO}_2$  concentration between 2 and 12  $\text{g/m}^2$  and results of  $\text{NO}_x$  degradation for the loadings are presented in Table 7. An increase of the activity with the loading is observed followed by a stabilization, which allows to highlight the optimal value of loading. Below this value, the activity does not increase if more  $\text{TiO}_2$  is added. Indeed, when the  $\text{TiO}_2$  layer has recovered the entire surface, an increase of the thickness does not allow to increase the activity because a part of  $\text{TiO}_2$  is not exposed to light and is not active. Furthermore, at this optimal loading (10  $\text{g/m}^2$  of  $\text{TiO}_2$ ),  $\eta_{\text{NO}_2}$  presents a minimum value (0.37), characteristic of a low amount of  $\text{NO}_2$  desorbed compared to the amount of NO degraded (Eq. 10): the lower the  $\eta_{\text{NO}_2}$ , the higher the reduction of  $\text{NO}_x$ .

The kinetic order is checked by following the reaction rate when the initial NO concentration is modified and the results are presented in Figure 11. The shape of the different curves (NO and  $\text{NO}_x$ ) is linear confirming the first order for the two reactions. The kinetic constants,  $k_{\text{NO}}$  and  $k_{\text{NO}_x}$ , are calculated from the slope of the curves and values of  $k_{\text{NO}} = 0.410 \text{ m/min}$  and  $k_{\text{NO}_x} = 0.208 \text{ m/min}$  are obtained. These values are the same order of magnitude than that found in the literature and even higher showing that the  $\text{TiO}_2$  coatings used in this work are much photoactive [13, 45].

All this characterizations show that  $\text{TiO}_2$  P25/E coating is deposited on different concrete substrates with success. This coating presents the best mechanical (abrasion) and freeze-thaw resistances

compared to the other coatings developed in this study. This coating is made with an industrializable process, which opens perspectives for road applications.

### 3.6. Comparison with literature

In this section, the coatings obtained in this study are compared to other studies dealing with photocatalytic application of  $\text{TiO}_2$  coatings, the difficulty of the comparison resides in the large range of conditions used in the various studies as the light intensity, the gas flow/contact time, the pollutant concentration, the substrate or the photocatalyst amount.

In Faraldo *et al.* [52], they use two different concrete substrates (concrete blocks and cement tiles) with  $\text{TiO}_2$ -based coatings (pure or mixed with  $\text{SiO}_2$ , Siloxane). The coatings are also assessed for the degradation of  $\text{NO}_x$ . With similar photocatalytic reactor, the coatings reach high conversion ( $\sim 95\%$ ). In this study, the conversion reaches 45% with the best coating (Table 3) but in this case, the gas flow is faster leading to smaller contact time, the coating thickness is also smaller and the  $\text{NO}_x$  concentration is lower which can be harder to degrade. In Faraldo *et al.* [52], no durability study or resistance to mechanical abrasion and freeze-thaw cycle is considered. In the review of Da Siva *et al.* [53], numerous information's are resumed about the  $\text{TiO}_2$  photocatalysts previously developed, the different deposition methods, the thermal treatment, their applications in photocatalytic reactions and their uses as photocatalytic coatings for ceramic tiles. The difficulty of comparison between all existing studies is highlighted. This review concludes that commercial products exist for photocatalytic applications but it is quite limited as the photocatalytic effect is not always clearly observed. The main important points are to obtain a crystalline  $\text{TiO}_2$  coating with durable properties with time, with the lowest possible costs and the highest photocatalytic performances. The adherence is a crucial parameter. In this work, the durability is clearly a parameter that was assessed with the mechanical resistance and freeze-thaw experiments. Also in this study, the syntheses of  $\text{TiO}_2$  colloids have been developed in the context of reducing their costs. In Murugan *et al.* [54], Patrocínio *et al.* [55] or Léonard *et al.* [27], different formulations of  $\text{TiO}_2$  coatings are investigated as self-cleaning coatings on glass. In these studies, the photocatalytic activity is also highlighted but the durability is not shown. The  $\text{TiO}_2$  materials are doped with  $\text{Ni}^{2+}$  [54],  $\text{Fe}^{3+}$  [54],  $\text{WO}_3$  [55] or  $\text{ZnO}$  [27] showing improvement in photocatalytic properties but

also leading to an increase of the cost for an industrial application. In this study, only pure TiO<sub>2</sub> coatings are evaluated to reduce the cost associated to the deposited material. In Onna *et al.* [56], W-TiO<sub>2</sub> coatings are developed for photocatalytic, antimicrobial and self-cleaning properties. This study shows the feasibility of the product at large scale (industrial plant) going a step further than laboratory development. With one coating of this work (TiO<sub>2</sub> AQ), it was also possible to produce large scale self-cleaning [11] and photocatalytic [57] coatings on steel substrate. All these studies show that the development of photocatalytic coatings based on TiO<sub>2</sub> materials is a research field where many challenges still exist in order to produce a material with very high performance at industrial scale, but promising solutions exist.

#### 4. Conclusions

In this study, six different coatings have been developed for photocatalytic application on roads. The coatings are synthesized by sol-gel process in organic or water solvent, by a functionalization technique with hydroxybenzoic acid on commercial Evonik P25 catalyst and by a Degussa patent using also commercial Evonik P25 catalyst. These suspensions are deposited by dip-coating or spray-coating on three different concrete substrates: pavement block, brushed or exposed aggregates concrete. For each process, particular attention was paid to the development of TiO<sub>2</sub> synthesis that will be easily produced on a larger scale.

The photocatalytic activity of all samples are tested on the degradation on NO<sub>x</sub> in gaseous phase. Excepted the samples resulting from the sol-gel organic route, all other samples show a NO<sub>x</sub> degradation between 10 and 45 %. So the coatings are photoactive on road pollutants. To choose the best candidate for further characterizations, mechanical abrasion and freeze-thaw resistance tests are performed. These tests show that the best coating is the TiO<sub>2</sub> P25/E coating synthesized by the functionalization of commercial Evonik P25 catalyst.

Additional characterizations on this coating highlight that anatase TiO<sub>2</sub> is well present at the surface of the sample giving a bright aspect of the surface when observed with profilometry. A study of

the  $\text{TiO}_2$  loading on the surface of concrete is made. This study shows that the photoactivity increases with the amount of  $\text{TiO}_2$  until an optimal value is reached where the activity stabilizes. Indeed, when the  $\text{TiO}_2$  layer covers all the surface, an increase of the thickness does not allow to increase the activity because a part of the  $\text{TiO}_2$  is not exposed to light and is not active.

The  $\text{TiO}_2$  P25/E coating shows good properties for road applications. However, further works have to be done in order to increase its abrasion resistance for applications in real conditions.

## **Acknowledgments**

S. D. L. thanks to the Belgian National Funds for Scientific Research (F.R.S.-FNRS) for her Senior Associate Researcher position. The authors also thank to the Ministère de la Région Wallonne Direction Générale des Technologies, de la Recherche et de l'Energie (DG06) and the Fond de Bay.

## **Compliance with ethical standards**

Conflict of interest: The authors declare that they have no conflicts of interest.

## **References**

- [1] M.A. Khan, A.M. Ghouri, ENVIRONMENTAL POLLUTION : Its effects on life and its remedies, *J. Arts, Sci. Commer.* 2 (2011) 276–285.
- [2] J. McGlade, Cet air que nous respirons Améliorer la qualité de l' air en Europe, Copenhague, 2013. doi:10.2800/84920.
- [3] Pollution atmosphérique, *Eur. Environ. Agency.* (2008), <https://www.eea.europa.eu/fr/themes/air/intro> (accessed June 2018).
- [4] J. Ângelo, L. Andrade, L.M. Madeira, A. Mendes, An overview of photocatalysis phenomena applied to  $\text{NO}_x$  abatement, *J. Environ. Manage.* 129 (2013) 522–539. doi:10.1016/j.jenvman.2013.08.006.

[5] A. Mills, S. Le Hunte, An overview of semiconductor photocatalysis, *J. Photochem. Photobiol. A Chem.* 108 (1997) 1–35. doi:10.1016/S1010-6030(97)00118-4.

[6] A. Fujishima, K. Hashimoto, T. Watanabe, *TiO<sub>2</sub> Photocatalysis: Fundamentals and Applications*, 1999.

[7] M.R. Hoffmann, S.T. Martin, W. Choi, D.W. Bahnemann, Environmental Applications of Semiconductor Photocatalysis, *Chem. Rev.* 95 (1995) 69–96. doi:10.1021/cr00033a004.

[8] C.M. Malengreux, S. Douven, D. Poelman, B. Heinrichs, J.R. Bartlett, An ambient temperature aqueous sol–gel processing of efficient nanocrystalline doped TiO<sub>2</sub>-based photocatalysts for the degradation of organic pollutants, *J. Sol-Gel Sci. Technol.* 71 (2014) 557–570. doi:10.1007/s10971-014-3405-6.

[9] O. CARP, Photoinduced reactivity of titanium dioxide, *Prog. Solid State Chem.* 32 (2004) 33–177. doi:10.1016/j.progsolidstchem.2004.08.001.

[10] M. A. Rauf, S.S. Ashraf, Fundamental principles and application of heterogeneous photocatalytic degradation of dyes in solution, *Chem. Eng. J.* 151 (2009) 10–18. doi:10.1016/j.cej.2009.02.026.

[11] J.G. Mahy, G.L.-M. Léonard, S. Pirard, D. Wicky, A. Daniel, C. Archambeau, et al., Aqueous sol-gel synthesis and film deposition methods for the large-scale manufacture of coated steel with self-cleaning properties, *J. Sol-Gel Sci. Technol.* 81 (2017) 27–35. doi:10.1007/s10971-016-4020-5.

[12] J.G. Mahy, S.D. Lambert, G.L.-M. Léonard, A. Zubiaur, P.-Y. Olu, A. Mahmoud, et al., Towards a large scale aqueous sol-gel synthesis of doped TiO<sub>2</sub>: Study of various metallic dopings for the photocatalytic degradation of p-nitrophenol, *J. Photochem. Photobiol. A Chem.* 329 (2016). doi:10.1016/j.jphotochem.2016.06.029.

[13] M.M. Ballari, M. Hunger, G. Hüskens, H.J.H. Brouwers, Modelling and experimental study of the NO<sub>x</sub> photocatalytic degradation employing concrete pavement with titanium dioxide, *Catal. Today.* 151 (2010) 71–76. doi:10.1016/j.cattod.2010.03.042.

[14] J. Victor, S. De Melo, G. Trichêes, P. Jean, P. Gleize, J. Villena, Development and evaluation of the efficiency of photocatalytic pavement blocks in the laboratory and after one year in the

field, *Constr. Build. Mater.* 37 (2012) 310–319. doi:10.1016/j.conbuildmat.2012.07.073.

[15] J. Chen, C. Poon, Photocatalytic construction and building materials : From fundamentals to applications, *Build. Environ.* 44 (2009) 1899–1906. doi:10.1016/j.buildenv.2009.01.002.

[16] E. Boonen, A. Beeldens, Photocatalytic roads : from lab tests to real scale applications, *Eur. Transp. Res. Rev.* (2013) 79–89. doi:10.1007/s12544-012-0085-6.

[17] S. Shen, M. Burton, B. Jobson, L. Haselbach, Pervious concrete with titanium dioxide as a photocatalyst compound for a greener urban road environment, *Constr. Build. Mater.* 35 (2012) 874–883. doi:10.1016/j.conbuildmat.2012.04.097.

[18] E. Boonen, A. Beeldens, I. Dirkx, V. Bams, Durability of Cementitious Photocatalytic Building Materials, *Catal. Today.* 287 (2017) 196–202. doi:10.1016/j.cattod.2016.10.012.

[19] C. d'études des Tunnels, ed., *Le traitement de l'air des tunnels routiers*, Bron, 2016.

[20] G.L. Guerrini, Photocatalytic performances in a city tunnel in Rome : NO x monitoring results, *Constr. Build. Mater.* 27 (2012) 165–175. doi:10.1016/j.conbuildmat.2011.07.065.

[21] A.M. Neville, *Properties of concrete*, Wiley, New York, 1995.

[22] D.M. Antonelli, J.Y. Ying, Synthesis of Hexagonally Packed Mesoporous TiO<sub>2</sub> by a Modified Sol–Gel Method, *Angew. Chemie Int. Ed. English.* 34 (1995) 2014–2017. doi:10.1002/anie.199520141.

[23] C. Anderson, A.J. Bard, An Improved Photocatalyst of TiO<sub>2</sub>/SiO<sub>2</sub> Prepared by a Sol–Gel Synthesis, *J. Phys. Chem.* 99 (1995) 9882–9885. doi:10.1021/j100024a033.

[24] M. Gratzel, Sol-gel processed TiO<sub>2</sub> films for photovoltaic applications, *J. Sol-Gel Sci. Technol.* 22 (2001) 7–13. doi:10.1023/A:1011273700573.

[25] J.G. Mahy, F. Deschamps, V. Collard, C. Jérôme, J. Bartlett, S.D. Lambert, et al., Acid acting as redispersing agent to form stable colloids from photoactive crystalline aqueous sol–gel TiO<sub>2</sub> powder, *J. Sol-Gel Sci. Technol.* 87 (2018) 568–583. doi:10.1007/s10971-018-4751-6.

[26] J.G. Mahy, V. Claude, L. Sacco, S.D. Lambert, Ethylene polymerization and hydrodechlorination of 1 , 2- dichloroethane mediated by nickel ( II ) covalently anchored to silica xerogels, *J. Sol-Gel Sci. Technol.* 81 (2017) 59–68. doi:10.1007/s10971-016-4272-0.

[27] G.L. Léonard, C.A. Pàez, A.E. Ramírez, J.G. Mahy, B. Heinrichs, Interactions between Zn<sup>2+</sup>

or ZnO with TiO<sub>2</sub> to produce an efficient photocatalytic, superhydrophilic and aesthetic glass, *J. Photochem. Photobiol. A Chem.* 350 (2018) 32–43. doi:10.1016/j.jphotochem.2017.09.036.

[28] G.W. Brinker, C. Jeffrey, Scherer, *Sol-gel science: the physics and chemistry of sol-gel processing*, Academic presse, 2013.

[29] C.M. Malengreux, G.M.-L. Léonard, S.L. Pirard, I. Cimieri, S.D. Lambert, J.R. Bartlett, et al., How to modify the photocatalytic activity of TiO<sub>2</sub> thin films through their roughness by using additives. A relation between kinetics, morphology and synthesis, *Chem. Eng. J.* 243 (2014) 537–548. doi:10.1016/j.cej.2013.11.031.

[30] D. Kapusuz, J. Park, A. Ozturk, Effect of initial water content and calcination temperature on photocatalytic properties of TiO<sub>2</sub> nanopowders synthesized by the sol – gel process, 41 (2015) 12788–12797. doi:10.1016/j.ceramint.2015.06.114.

[31] C.M. Malengreux, A. Timmermans, S.L. Pirard, S.D. Lambert, J.-P. Pirard, D. Poelman, et al., Optimized deposition of TiO<sub>2</sub> thin films produced by a non-aqueous sol–gel method and quantification of their photocatalytic activity, *Chem. Eng. J.* 195–196 (2012) 347–358. doi:10.1016/j.cej.2012.04.076.

[32] U. Schubert, Chemical modification of titanium alkoxides for sol–gel processing, *J. Mater. Chem.* 15 (2005) 3701. doi:10.1039/b504269k.

[33] K.M.S. Khalil, R.M. El-Khatib, T.T. Ali, H.A. Mahmoud, A.A. Elsamahy, Titania nanoparticles by acidic peptization of xerogel formed by hydrolysis of titanium(IV) isopropoxide under atmospheric humidity conditions, *Powder Technol.* 245 (2013) 156–162. doi:10.1016/j.powtec.2013.04.023.

[34] C. Leyva-Porras, A. Toxqui-Teran, O. Vega-Becerra, M. Miki-Yoshida, M. Rojas-Villalobos, M. García-Guaderrama, et al., Low-temperature synthesis and characterization of anatase TiO<sub>2</sub> nanoparticles by an acid assisted sol–gel method, *J. Alloys Compd.* 647 (2015) 627–636. doi:10.1016/j.jallcom.2015.06.041.

[35] S. Mahshid, M. Askari, M.S. Ghamsari, Synthesis of TiO<sub>2</sub> nanoparticles by hydrolysis and peptization of titanium isopropoxide solution, *J. Mater. Process. Technol.* 189 (2007) 296–300.

doi:10.1016/j.jmatprotec.2007.01.040.

- [36] S. Hore, E. Palomares, H. Smit, N.J. Bakker, P. Comte, P. Liska, et al., Acid versus base peptization of mesoporous nanocrystalline TiO<sub>2</sub> films: functional studies in dye sensitized solar cells, *J. Mater. Chem.* 15 (2005) 412. doi:10.1039/b407963a.
- [37] C.J. Barbe, F. Arendse, P. Comte, M. Jirousek, F. Lenzmann, V. Shklover, et al., Nanocrystalline Titanium Oxide Electrodes for Photovoltaic Applications, 71 (1997) 3157–3171.
- [38] C.A. Páez, D. Liquet, C. Calberg, D. Eskenazi, J.-P. Pirard, B. Heinrichs, Patent WO2013171297A2, (2013).
- [39] J.G. Mahy, V. Cerfontaine, D. Poelman, F. Devred, E.M. Gaaigneaux, B. Heinrichs, et al., Highly efficient low-temperature N-doped TiO<sub>2</sub> catalysts for visible light photocatalytic applications, *Materials (Basel)*. 11 (2018). doi:10.3390/ma11040584.
- [40] G.L.-M. Léonard, C.M. Malengreaux, Q. Mélotte, S.D. Lambert, E. Bruneel, I. Van Driessche, et al., Doped sol–gel films vs. powders TiO<sub>2</sub>: On the positive effect induced by the presence of a substrate, *J. Environ. Chem. Eng.* 4 (2016) 449–459. doi:10.1016/j.jece.2015.11.040.
- [41] J. Moser, S. Punchihewa, P.P. Infelta, M. Grätzel, Surface Complexation of Colloidal Semiconductors Strongly Enhances Interfacial Electron-Transfer Rates, *Langmuir*. 7 (1991) 3012–3018. doi:10.1021/la00060a018.
- [42] K. Wu, Y. Wang, I. Zhitomirsky, Electrophoretic deposition of TiO<sub>2</sub> and composite TiO<sub>2</sub>-MnO<sub>2</sub> films using benzoic acid and phenolic molecules as charging additives, *J. Colloid Interface Sci.* 352 (2010) 371–378. doi:10.1016/j.jcis.2010.08.059.
- [43] Y. Deng, M. Oswald, K. Deller, *Aqueous/Organic Metal Oxide Dispersion And Coated Substrates And Mouldings Produced Therewith*, 2008.
- [44] R. numberISO 22197-1:2007(E), ISO 22197-1. Fine ceramics (advanced ceramics, advanced technical ceramics)– Test method for air-purification performance of semi conductingphotocatalytic materials – Part 1: Removal of nitric oxide., Switzerlan (2007).
- [45] C. Minero, A. Bedini, M. Minella, On the Standardization of the Photocatalytic Gas / Solid Tests, *Int. J. Chem. React. Eng.* 11 (2013) 717–732. doi:10.1515/ijcre-2012-0045.

[46] European Standard - BS EN 1097-8:2009 Tests for mechanical and physical properties of aggregates. Determination of the polished stone value, 2009.

[47] Aggregate test, NorthStone Ltd. Quarr. Asph. Div.,  
[http://www.northstonematerials.com/aggregate\\_test](http://www.northstonematerials.com/aggregate_test) (accessed May 31, 2017)..

[48] Technical Specification - TS 12390-9 : Testing hardened concret - part 9 : Freezethaw resistance - scaling, 2006.

[49] J.G. Mahy, C.A. Paez, C. Carcel, C. Bied, A.S. Tatton, C. Damblon, et al., Porphyrin-based hybrid silica-titania as a visible-light photocatalyst, *J. Photochem. Photobiol. A Chem.* 373 (2019) 66–76. doi:10.1016/j.jphotochem.2019.01.001.

[50] K. Wang, D.E. Nelsen, W.A. Nixon, Damaging effects of deicing chemicals on concrete materials, *Cem. Concr. Compos.* 28 (2006) 173–188. doi:10.1016/j.cemconcomp.2005.07.006.

[51] C.J. Engelsen, G. Wibetoe, H.A. Van Der Sloot, W. Lund, G. Petkovic, Field site leaching from recycled concrete aggregates applied as sub-base material in road construction, *Sci. Total Environ.* 427–428 (2012) 86–97. doi:10.1016/j.scitotenv.2012.04.021.

[52] M. Faraldo, R. Kropp, M.A. Anderson, K. Sobolev, Photocatalytic hydrophobic concrete coatings to combat air pollution, *Catal. Today.* 259 (2016) 228–236.  
doi:10.1016/j.cattod.2015.07.025.

[53] A.L. Da Silva, M. Dondi, M. Raimondo, D. Hotza, Photocatalytic ceramic tiles: Challenges and technological solutions, *J. Eur. Ceram. Soc.* 38 (2018) 1002–1017.  
doi:10.1016/j.jeurceramsoc.2017.11.039.

[54] M. Murugan, R. Subasri, T.N. Rao, A.S. Gandhi, B.S. Murty, Synthesis, characterization and demonstration of self-cleaning TiO<sub>2</sub> coatings on glass and glazed ceramic tiles, *Prog. Org. Coatings.* 76 (2013) 1756–1760. doi:10.1016/j.porgcoat.2013.05.012.

[55] A.O.T. Patrocinio, L.F. Paula, R.M. Paniago, J. Freitag, D.W. Bahnemann, Layer-by-Layer TiO<sub>2</sub> /WO<sub>3</sub> Thin Films As Efficient Photocatalytic Self- Cleaning Surfaces, *ACS Appl. Mater. Interfaces.* 6 (2014) 16859–16866.

[56] D. Onna, K.M. Fuentes, C. Spedalieri, M. Perullini, M.C. Marchi, F. Alvarez, et al., Wettability, Photoactivity, and Antimicrobial Activity of Glazed Ceramic Tiles Coated with

Titania Films Containing Tungsten, ACS Omega. 3 (2018) 17629–17636.

doi:10.1021/acsomega.8b03339.

[57] J.G. Mahy, S.D. Lambert, J. Geens, A. Daniel, D. Wicky, C. Archambeau, et al., Large scale production of photocatalytic TiO<sub>2</sub> coating for volatile organic compound (VOC) air remediation, AIMS Mater. Sci. 5 (2018) 945–956. doi:10.3934/matersci.2018.5.945.